ELSEVIER

Two-stages optimised design of the collector field of solar power tower plants

CrossMark

Francisco J. Collado *, Jesus Guallar

Department of Mechanical Engineering, EINA, Universidad de Zaragoza, María de Luna 3, 50018 Zaragoza, Spain

ABSTRACT

In solar power tower (SPT) systems, selecting the optimum location of thousands of heliostats and the most profitable tower height and receiver size remains a challenge. Given the complexity of the problem, breaking the optimisation process down into two consecutive steps is suggested here; first, a primary, or energy, optimisation, which is practically independent of the cost models, and then a main, or economic, optimisation. The primary optimisation seeks a heliostat layout supplying the maximum annual incident energy for all the explored combinations of receiver sizes and tower heights. The annual electric output is then calculated as the combination of the incident energy and the simplified (annual averaged) receiver thermal losses and power efficiencies. Finally, the figure of merit of the main optimisation is the levelised cost of electric energy (LCOE) where the capital cost models used for the LCOE calculation are reported by the System Advisor Model (SAM)-NREL and Sandia. This structured optimisation, splitting energy procedures from economic ones, enables the organisation of a rather complex process, and it is not limited to any particular power tower code. Moreover, as the heliostat field layout is already fully optimised before the economic optimisation, the profiles of the LCOE versus the receiver radius for the tower heights explored here are sharp enough to establish optima easily. As an example of the new procedure, we present a full thermo-economic optimisation for the design of the collector field of an actual SPT system (Gemasolar, 20 MWe, radially staggered surrounding field with 2650 heliostats, 15 h of storage). The optimum design found for Gemasolar is reasonably consistent with the scarce open data. Finally, optimum designs are strongly dependent on the receiver cost, the electricity tariff and the assumed maximum receiver surface temperature.

© 2016 The Author(s). Published by Elsevier Ltd. This is an open access article under the CC BY-NC-ND license (http://creativecommons.org/licenses/by-nc-nd/4.0/).

1. Introduction

Solar power tower systems are currently booming, since several new projects at a commercial scale (>100 MWe) have entered the construction phase worldwide (SolarPACES, 2016). At such a scale, the levelised cost of energy (LCOE) of power tower systems should definitely be reduced to compete with fossil power plants.

The collector field, with thousands of heliostats or giant mirrors concentrating sunlight onto a receiver atop a tower, is the central building block for solar tower plants (Kolb et al., 2011; Kolb, 2011). However, unfortunately, the optimum design of the collector field of such plants remains a challenge, mainly due to the difficulties in heliostat field layout optimisation, with thousands of mirrors, combined with the simultaneous search for optimum values for the tower height, receiver size, and so on, giving the lowest LCOE.

In the open literature, DELSOL3 from Sandia Labs (Kistler, 1986) (originally written in 1986) has become practically a standard (Kolb, 2011; Avila-Marin et al., 2013) in current power tower codes that are able to perform a thermo-economic optimised design of the collector field based on LCOE. The code HFLCAL from German DLR (Schmitz et al., 2006; Schwarzbölz et al., 2009) is also a fully optimised code for solar tower plants but the details about it are rather scarce.

However, DELSOL3 exhibits several drawbacks mainly due to the rather limited computer capacities in the eighties. First, it makes some major simplifications about annual performances, in particular, the division of the whole field into 11×11 cells (with numerous heliostats in each one). Consequently, detailed performance factors are usually only calculated for the heliostat in the centre of the cell. Moreover, the optimum layouts were previously found in the 1980s through cost-energy optimisations using the RCELL code (Lipps and Vant-Hull, 1978). Finally, and probably as a result of these simplifications, the LCOE minima profiles in DELSOL3 are shallow, see page 118 in Kistler (1986), thus there are no clear selection criteria.

Nowadays, with the huge calculation power of current personal computers, the question is if a much more detailed performance analysis of the heliostat field (heliostat by heliostat) would provide LCOE profiles sharp enough to establish clear minima. So that, the reliability of such optimised designs would be greatly increased.

Furthermore, the optimisation could be based on an advanced search algorithm such as genetic algorithms. In that case, the tower height, receiver size, and the layout parameters are the design variables and LCOE is the single objective function.

However, a detailed annual performance of thousands of heliostats for a large amount of feasible layouts, with a lot of choices for tower height and receiver size, in addition to the uncertainty of the current cost models, etc., raises major issues with regard to the above search algorithm. In particular, how we could efficiently manage tens of layout options matching them with the LCOE along the optimisation, which would be the range of variation of the design variables and the most convenient variation step, etc. Using the language of genetic algorithms (Obitko, 2016), we could say that the search space (each point in the search space represent one feasible solution) is, by the moment, rather diffuse.

Therefore, in this work, it is suggested to break the optimisation down into two consecutive steps: first, a primary, or energetic, optimisation, which is practically independent of the cost models, and then a main, or economic, optimisation. The primary optimisation would seek a heliostat layout supplying the maximum annual incident energy for all the explored combinations of receiver sizes and tower heights.

It is necessary to highlight that the optimisation decomposition could exhibit some disadvantages. The most important one would be that it is not guaranteed to give an optimal solution of the overall problem.

However, supporting this phased optimisation approach, several detailed layout optimisation codes, which only optimise the heliostat field layout based on receiver size and tower height, have emerged in recent years (Sánchez and Romero, 2006; Wei et al., 2010; Noone et al., 2012; Collado and Guallar, 2013; Besarati and Goswami, 2014; Atif and Al-Sulaiman, 2015). Some of these layout codes published before 2012 (Sánchez and Romero, 2006; Wei et al., 2010; Noone et al., 2012) were reviewed in Collado and Guallar (2013).

This last work is also the layout optimisation, through a smart search, of a surrounding radially staggered heliostat field giving the maximum yearly insolation weighted efficiency, or maximum field efficiency, for a Gemasolar-like 20 MWe plant with 2650 heliostats. The tower optical height and the receiver radius were set to $THT = 130$ m and $RR = 4$ m, respectively. Only two design variables, namely constant radial increments between consecutive rows for the second and third zones, respectively, could define the whole layout of the regular concentric rings generated heliostat field.

Along the same lines, Besarati and Goswami (2014) have recently studied layout optimisation, based on genetic algorithms, of a 50 MWth heliostat field (with a cavity receiver) to provide the maximum field efficiency for Dagget, California, where the shape of the biomimetic spiral pattern-based layout (Noone et al., 2012) is defined by only two design variables. The specific field parameters used along the optimisation were $THT = 115$ m, a receiver aperture width of 13.78 m, and an aperture height of 12 m.

Atif and Al-Sulaiman (2015) have also recently performed a layout optimisation (maximum field efficiency), using differential evolution algorithms, for a regular surrounding radially staggered field with 2940 heliostats located in Dhahran city, Saudi Arabia. Here, the prescribed field parameters are $THT = 130$ m with a receiver diameter $DR = 9.44$ m. The four layout design variables the optimisation determines are an increment of the maximum heliostat footprint, which controls the angular distance between adjacent heliostats in the first ring in each zone, and the three radial spaces between the rows of the heliostats for each of the three zones defined.

Until the knowledge of the authors, LCOE profiles calculated with any of these recent codes have neither published nor even suggested how to use this layout codes to perform a LCOE optimisation of the collector field.

The logic next phase proposed here should be to energetically optimise the layout but now for several sets of design variables (THT, RR) chosen around a reference case. However, all of them need to have the same prescribed number of heliostats N_{hel} to keep the heliostat cost virtually constant so that the whole problem could be effectively broken into two simpler ones. After this primary optimisation, several design collector fields $(THT, RR, corresponding\ optimum\ layout)$, all of them giving a maximum annual energy, would be available prior to their LCOE calculations. Finally, the LCOE (the levelised cost-net annual energy ratio) of the various design options is the figure of merit of the economic optimisation.

The reference collector field used to check the new procedure is that of Gemasolar (Vázquez et al., 2006; Lata et al., 2006, 2010; Ortega et al., 2006; Burgaleta et al., 2011; Relloso and Lata, 2011), the first solar power tower commercial plant (19.9 MWe, N_{hel} = 2650 heliostats) with molten salt storage (15 h) in the world. The layout code used is *campo* (Collado and Guallar, 2013) although the simple parametric analysis suggested here is not limited to a particular layout code, or even a specific layout pattern, as it is perfectly reproducible by any of the above-commented layout codes.

Finally, the structure of this work is as follows. Section 2 introduces the primary layout optimisation for every set of design variables (THT, RR) checked here, namely 5×5 combinations. The minimum set of variables that reproduce the whole layout is briefly reviewed and how they should be varied along the search is analysed. Some details of the field efficiency are gathered in electronic pdf file Appendix A whereas some comments about the optimal layouts is presented in Appendix B. The energy performances of the twenty-five designs are then available. Section 3 calculates the net annual energy output E_E for those designs. The Sandia (Kistler, 1986) annual energy bookkeeping has been followed, in which the annual receiver thermal losses and the thermodynamic cycle efficiency are assumed to be constant. Section 4 reviews the LCOE economic terms and the investment cost models of the main collector field equipment. Section 5 combines the net annual energy E_E with capital cost models to plot the sensitivity of the LCOE against various design and cost options searching minima. Finally, Section 6 discusses the main assumptions and advantages of the new proposed optimum search, and provides some conclusions.

2. Primary optimisation of the field layout for every (THT, RR) considered

2.1. Field efficiency

For every (THT, RR) considered, several layout design options for $N_{hel} = 2650$ are tested. The corresponding optimal layout should give a local maximum of the optical (annual averaged) field efficiency η_{field}. The factors that set up the optical efficiency of a heliostat are classically defined in Pacheco et al. (2000), Pacheco (2002) whereas the mathematical models used by *campo* to calculate such factors have been defined elsewhere (Collado and Guallar, 2013, 2012; Collado, 2010; Sassi, 1983). Then, only a brief summary is presented in the electronic Appendix A. *Field efficiency*. As in Collado and Guallar (2013), due to a lack of data, a typical meteorological year (TMY) for PSA (Almería) Meinecke, 1982, which has similar latitude to Gemasolar, is used.

2.2. Reducing the number of design variables for radially staggered layouts

The procedure followed by *campo* to generate a regular radially staggered layout has been explained in detail elsewhere (Collado and Guallar, 2012). Thus, only the more relevant assumptions are briefly commented here.

The maximum footprint of any heliostat is a circle with a diameter DM equal to its diagonal DH, which for Sener heliostats used in Gemasolar (Vázquez et al., 2006; Lata et al., 2010) is 15.70 m, plus any additional security distance $dsep$, $DM = DH + dsep$. In (Collado and Guallar, 2013), $dsep = 0$.

The number of heliostats of the first row in the first zone, closest to the tower, is $Nhel_1 = 46$, whose footprint circles are tangential each other. This value of $Nhel_1$ was based on the DELSOL3 recommendation that the radius of the first row is of the order of $0.75 * THT$. So, the radius of the first heliostat row is $R_1 = (DM \cdot Nhel_1)/2\pi = 114.94$ m, which is 88% of 130 m (the tower height reference) but about 80% of 140 m.

The azimuth angular spacing for each zone is kept constant to strictly maintain the radially staggered pattern. Then, the number of heliostats per row for each zone does not change along the optimisation.

However, the length of the azimuth spacing (metres) between adjacent heliostats will accordingly increase with the radius of the row. This gives a criterion to finish any zone: when an extra heliostat can be placed between two adjoining mirrors in the same row. Thus, the azimuth angular spacing of the next outer zone will be half the previous one whereas the number of heliostats per row will be doubled. For a Gemasolar-like field we have three zones (Collado and Guallar, 2013).

On the other hand, the minimum radial increment between consecutive rows is $\Delta R_{min} = DM \cdot \cos 30^\circ = 0.866 \cdot DM$. Indeed, for zone 1, the optimum radial increment always resulted in the minimum distance, $\Delta R_1 = \cos 30^\circ DM$ (Collado and Guallar, 2013). So, it is also true in this work.

Except for zone 1, the radial increments, constant for each zone, vary throughout layout optimisation. For convenience, the radial distances between sequential rows ΔR were put in DM units; therefore, $\Delta r_i = \Delta R_i/DM$, where sub-index i refers to any of the zones in the field.

In Collado and Guallar (2013), $dsep$ is chosen to be equal to zero since, as we need to increase the radial increments of zone 2 and zone 3 in searching the optimum layout, the actual starting radii of the second and third zones are certainly longer than the theoretical (minimum) ones. Therefore, although $dsep = 0$, the footprint circles of the heliostats at the first row of zones 2 and 3 are not at all tangential to each other thus an additional security distance is naturally included. Besides, the distance between any zone and the next outer zone is considered equal to the radial increment of the outer zone.

The convenience of setting $dsep$ to zero is confirmed in this work, which highlights the better performance of denser fields in zone 2 although more expanded ones in zone 3. However, higher the radius (zone 3), higher the length of the azimuth spacing (metres) between adjacent heliostats then higher the 'natural' additional distance added.

In short, for a Gemasolar-like plant and based on previous analysis (Collado and Guallar, 2013), we consider that $dsep = 0$, $Nhel_1 = 46$ and $\Delta r_1 = \cos 30^\circ$. Therefore, the layout of thousands of heliostats is defined completely using only the two remaining design variables, namely the non-dimensional constant radial increments of zone 2 and zone 3, Δr_2 and Δr_3, respectively.

Finally, the boundary of the field is the result of applying the condition that only the first 2650 heliostats with the best performance will be selected in the end. To correctly make this selection, which defines the trimming of the boundary, we have followed the HFLCAL procedure (Schmitz et al., 2006), which starts off with a larger field of heliostats, 3864.

2.3. Range of variation and step for the collector field design variables along the layout optimisations

2.3.1. Tower height and receiver radius around a reference case

In Collado and Guallar (2013), the optimum layout for only one design set i.e., the reference case ($THT = 130$ m, $RR = 4.0$ m), was explored. Here, we take the problem much further because now the optical tower height and receiver size are included in the optimisation. Based on Ortega et al. (2006) and on comprehensive groundwork, a total of five values around the former reference case have been finally considered here for RR and THT, respectively, namely $RR(m) = [3.0, 3.5, 4.0, 4.5, 5.0]$ and $THT(m) = [120, 130, 140, 150, 160]$. These total twenty-five basic combinations of THT and RR, which will be the core of the main optimisation.

Facing the energetic optimisation of the collector field, it is necessary to point out that as significant as the selection of the range of variation of these design variables is that of their variation steps. Indeed, the arising of clear optima in the LCOE profiles would be the best indicator of the suitability of the ranges and steps chosen.

2.3.2. Improved designs with new intervals of layout variables

In Collado and Guallar (2013), the preliminary optimum layout, only found for the reference case, was $\Delta r_2 = 1.4$, $\Delta r_3 = 2.0$.

However, after many subsequent runs, it has been definitely checked that the field performance clearly improves with denser fields in the second zone i.e., $\Delta r_2 \approx 1.1$, and with more expanded fields in the third zone ($\Delta r_3 \approx 2.2-2.4$).

Therefore, in this work, the scanned values of Δr_2 and Δr_3 have been appropriately changed from the ones used in Collado and Guallar (2013). Hence, nine combinations ($\Delta r_2, \Delta r_3$) were proven, in particular $\Delta r_2 = [1.0, 1.1, 1.2]$ and $\Delta r_3 = [2.0, 2.2, 2.4]$.

In conclusion, for every one of the twenty-five design variables sets (THT, RR) we selected, nine possible layout combinations ($\Delta r_2, \Delta r_3$) for $N_{hel} = 2650$ heliostats were checked, amounting to a total of 9×25 tested collector field designs ($layout, THT, RR$). Thus, the *campo* code is executed 225 times to obtain the corresponding η_{field} values.

Point out that arriving at a global optimum is neither currently necessary nor convenient, as merely one optimal layout (out of a total of nine combinations) has to be found for every one of the twenty-five pairs (THT, RR). Remember that this energetic optimisation is followed by an economic optimisation, in which a cost-energy ratio is going to be minimised. So, collector fields with high towers and big receivers (high optical performances) would not necessarily give a minimum LCOE.

2.4. Results of the primary layout optimisation for the analysed (THT, RR) sets

In the electronic pdf file entitled Appendix B. *Optimal layouts found*, Table B.1 gathers the resulting optimal layout design ($\Delta r_2, \Delta r_3$), with the highest η_{field}, for the twenty-five (THT, RR) design sets. The details of how these optimal layouts have been sought are explained in Figs. 1 and 2, which also confirm the adequacy of the variation intervals and steps selected for the layout variables.

Fig. 1 shows field efficiency η_{field} in function of the radial increment in zone 3 although, for the sake of clarity, for only nine
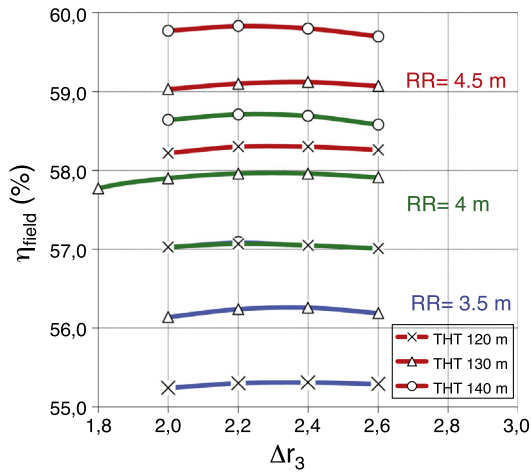
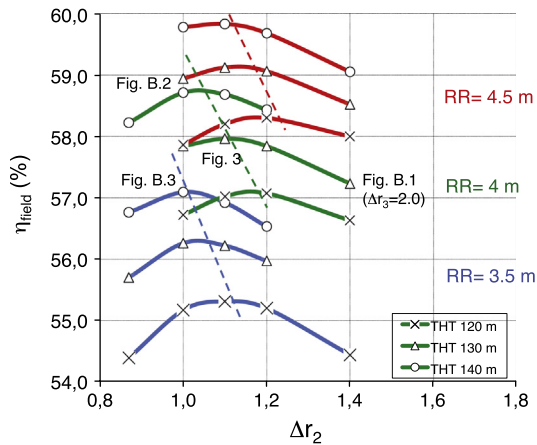**Fig. 1.** Field efficiency vs. Δr_3 for the optimum Δr_2 found.

Fig. 2. Field efficiency vs. Δr_2 for the optimum Δr_3 found.

combinations of the THT and RR. For each curve $\eta_{field}(\Delta r_3)$, the Δr_2 included supplies the maximum field efficiency for each (THT, RR) couple checked.

It is clear that the $\eta_{field}(\Delta r_3)$ curves found are extremely flat along the entire Δr_3 interval, independently of the given input set. This explains the two values of Δr_3 arising in Table B.1 for some cases.

However, see Fig. 2, the η_{field} optima curves in function of Δr_2 (also for the more efficient Δr_3) are clearly more acute than before. In Table B.1, such optima lie between $\Delta r_2 = 1.0$ and $\Delta r_2 = 1.2$ for almost all the design sets shown.

From these figures, it is clear that the layout optimisation is much more sensitive to Δr_2 variations than to Δr_3 ones. For subsequent designs, this could open the option that the layout optimisation practically depended on only one variable namely, Δr_2.

On the other hand, as example of the better performance of fields with denser zone 2 and more expanded zone 3, Fig. 3 shows the map of the individual annual averaged optical efficiency, $\eta_{annual}(x, y)$ for the reference case with the improved layout i.e., $\Delta r_2 = 1.1$ and $\Delta r_3 = 2.4$, in which $\eta_{field} = 57.96\%$. This figure should be compared with Fig. B.1 (Appendix B), which also shows the annual efficiency map for the reference case but here with the old layout design ($\Delta r_2 = 1.4, \Delta r_3 = 2.0$), ($\eta_{field} = 57.23\%$).

Furthermore, in Appendix B, the annual efficiency map of Fig. B.2 may be compared with that of Fig. B.3 where they have the same layout but different design sets. The boundary trimming

of all these fields is also very different although they have the same number of heliostats ($N_{hel} = 2650$).

Finally, for these optimum layouts in Table B.1, Fig. 4 depicts their corresponding optimum η_{field} versus receiver radius RR for the five tower heights THT scanned. In addition to the optimum layouts, these curves would be the main result of this primary, or energetic, optimisation.

Comment that, in Fig. 4, the field efficiency is clearly more sensitive to changes in the receiver radius than in tower height, although the larger the receiver, the lower the efficiency improvement in increasing the receiver size. Moreover, highlight that, from Eq. (A3) in Appendix A, a maximum η_{field} is equivalent to a maximum annual incident energy E_{inc} for a prescribed number of heliostats.

3. Net annual energy output E_E following DELSOL3 system optimisation

The net annual energy output E_E(kW h$_{el}$), which is the denominator of the LCOE, is calculated for the twenty-five collector field designs analysed in the above section.

3.1. Annual energy absorbed by the molten salts absorb at the receiver E_{abs}

First, the annual gross receiver energy (Kistler, 1986), or annual incident energy onto the receiver, is calculated

$$E_{inc} = A_m N_{hel} DNI \eta_{field} = E_{DNI} \eta_{field} \qquad (1)$$

where A_m is the mirror area of an individual heliostat, N_{hel} is the number of heliostats in the field (2650 for Gemasolar) and DNI is the annual direct normal insolation based on data for PSA Almería (Meinecke, 1982). The product $A_m \times N_{hel} \times DNI$ is the annual direct solar energy E_{DNI} over the heliostat field. See Appendix A.

Following (Kistler, 1986; Pacheco et al., 2000; Pacheco, 2002), the value of E_{inc} is used to subtract out annual receiver losses $L_{thermal}$ (receiver radiation and convection losses). The annual energy the molten salts absorb at the receiver E_{abs} Kistler, 1986; Ortega et al., 2006; Pacheco, 2002; Ho and Iverson, 2014 is

$$E_{abs} = \alpha_s \cdot E_{inc} - L_{thermal} = \eta_{rec} E_{inc} \Rightarrow \eta_{rec} = \frac{E_{abs}}{E_{inc}} = \alpha_s - \frac{L_{thermal}}{E_{inc}}, \qquad (2)$$

where α_s is the receiver solar absorptance of the tube panels (Kistler, 1986; Ortega et al., 2006; Pacheco, 2002; Ho and Iverson, 2014) and η_{rec} is the annual average receiver efficiency namely, the ratio of the annual energy the working fluid absorbs to the annual energy incident on the receiver (Pacheco, 2002).

3.2. Receiver efficiency and thermal losses

As a first approximation and based on Kistler (1986) and Pacheco (2002), the hourly and seasonal variation of thermal losses are assumed negligible. In order to calculate the losses, under steady state conditions, the temperature distributions on the receiver surface were also independent of the power level. This allows the approximation that the range of temperature operation gives an annual average wall temperature T_{wall}.

Clearly these assumptions are not true. For example, see temperature maps in function of the power level for the Solar Two receiver that Rodriguez-Sanchez et al. (2015) recently worked out.

However, by convenience, it would be valid to define an annual average mean wall receiver temperature T_{wall}, whose associated annual thermal losses were equal to the real ones, which are actually variable in time and space. Theoretically, it would be possible to get this T_{wall} through a detailed calculation of the wall
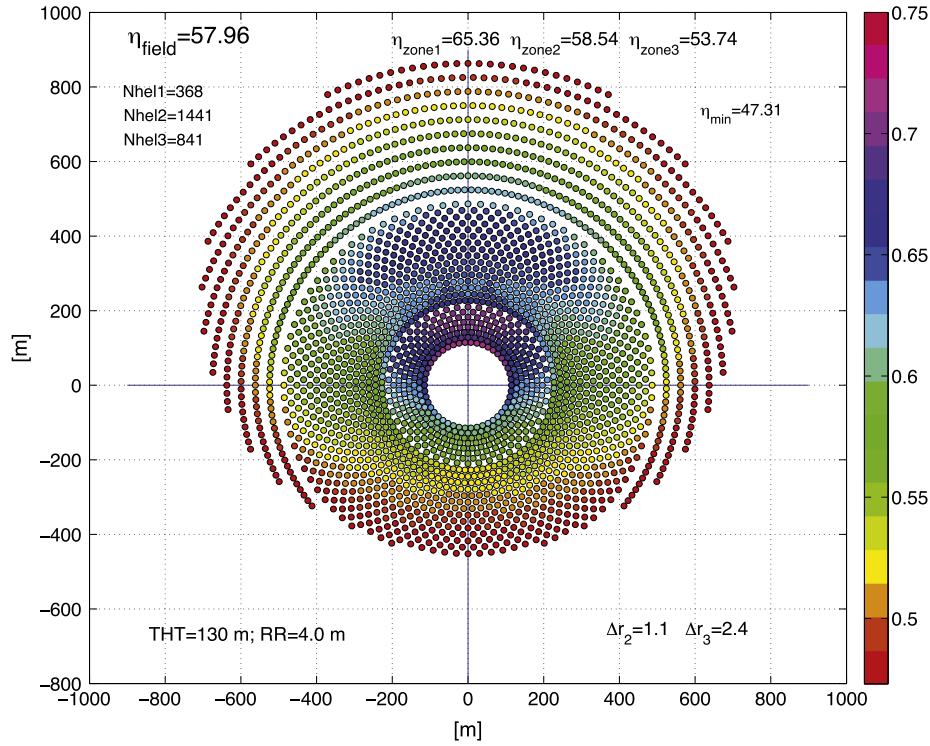
Fig. 3. Map of the annual efficiency for $\Delta r_2 = 1.1$ and $\Delta r_3 = 2.4$. THT = 130.00 m and RR = 4.00 m.
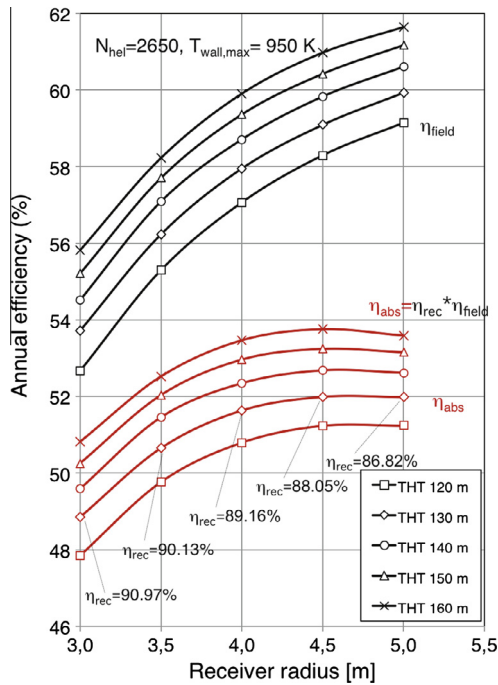

Fig. 4. Field efficiency and absorbed efficiency versus receiver radius (RR). THT = [120–160] m.

temperature maps for all the instants of time included in the TMY although, obviously, this would add a whole layer of complexity to the optimisation. This will be discussed later.

Here, as a first approach, a reasonable range of values is suggested for T_{wall}.

Therefore, the expression of the annual thermal losses, in which the individual losses for radiation and forced and natural

convection are calculated separately and summed, is (Kistler, 1986; Boehm, 1986)

$$
\begin{aligned}
L_{thermal} &= (Q_{rad} + Q_{conv})N_{hours} \\
&= [\varepsilon\sigma A_R(T_{wall}^4 - T_{amb}^4) + h_{mix}A_R(T_{wall} - T_{amb})]N_{hours}
\end{aligned}
\tag{3}
$$

where ε is the total hemispherical emittance (Kistler, 1986; Ho et al., 2014), σ is the Stefan–Boltzmann constant (5.67×10^{-8} W/m^2 K^4), A_R is the lateral surface of the cylindrical receiver (m^2), T_{wall} is the annual average mean wall receiver temperature (K), T_{amb} the ambient air temperature (here assumed to be about 293 K), h_{mix} a mixed convection coefficient, which is a combination of forced and natural mechanisms of convection (Kistler, 1986), and N_{hours} the real sunshine hours of the TMY used in this paper, 2789.8 h for Almeria using meteorological GAST data from the 1980s (Meinecke, 1982).

Then, receiver efficiency η_{rec}, substituting Eq. (3) in Eq. (2), is

$$
\begin{aligned}
\eta_{rec} &= \alpha_s - \frac{(Q_{rad} + Q_{conv})N_{hours}}{E_{inc}} \\
&= \alpha_s - \frac{[\varepsilon\sigma(T_{wall}^4 - T_{amb}^4) + h_{mix}(T_{wall} - T_{amb})]N_{hours}}{N_{hel}A_m DNI} \frac{A_R}{\eta_{field}},
\end{aligned}
\tag{4}
$$

which also includes Eq. (1).

The lateral area A_R of the receiver (a cylinder) can be approximated to a simple function of the receiver radius RR. Assuming as before (Ortega et al., 2006; Pacheco et al., 2000) that $HR \approx 2RR + 1$ then

$$
A_R \approx 2\pi RR\,(2RR + 1)
\tag{5}
$$

In conclusion, to calculate the annual receiver efficiency, Eq. (4), we would need the receiver solar absorptance α_s, the receiver hemispherical emittance ε, a representative wall receiver temperature T_{wall}, and the mixed convection coefficient h_{mix} for the Gemasolar

receiver (Vázquez et al., 2006; Lata et al., 2006; Ortega et al., 2006; Lata et al., 2010; Burgaleta et al., 2011; Relloso and Lata, 2011).

Concerning solar absorptance α_s, for a preliminary Sener design of the Gemasolar receiver it is reported (Lata et al., 2006) that the reflected power is 8.2 MW$_t$ at the design point for an incident power of 137.4 MW$_t$. Thus, solar absorptance would be $\alpha_s = 1-(8.2/137.4) = 0.9403$. This is the figure used here. Recent Sandia measurements of the Pyromark 2500 paint (Ho et al., 2014) confirm that $\alpha_s \approx 0.95$.

For emittance ε, the default value used in DELSOL3 (Kistler, 1986) is $\varepsilon = 0.90$. Sandia measurements (Ho et al., 2014) also confirm that the emittance is $\varepsilon \approx 0.88-0.89$ for a wall temperature of about 600 °C. In conclusion, a conservative value of $\varepsilon \approx 0.90$ is finally taken.

Regarding the annual average mean wall temperature of the receiver T_{wall}, a reasonable range is needed.

The basic assumptions are two: the first is uniform heat flux onto the receiver, which is the approximate result of the heliostats aim strategy; while the second is a constant convective coefficient between the molten salts and the inner tube wall (assuming turbulent flow and neglecting entry effects). Then, both the salts and the wall temperatures rise in parallel following a linear profile.

Hence, the wall peak temperature would be at the tube outlet and the minimum one would be at the inlet whereas the arithmetic mean of these two extreme values is the chosen T_{wall}.

The outlet temperature of the molten salts in Gemasolar is set to 838 K, whereas the inlet temperature is 563 K (Relloso and Lata, 2011). From a Sener preliminary receiver design (Lata et al., 2006), a wall peak temperature interval of around $T_{wall,max} \approx 1000-950$ K is estimated here to avoid an excessive pressure drop in the riser.

Thus, the difference between the latter and the molten salts outlet temperature would be $\Delta T \approx 950-838 = 112$ K so the inlet metal temperature would be around $563 + 112 = 675$ K.

Therefore, the mean wall temperature, used in the thermal losses, could be between $T_{wall} \approx 813-863$ K (according to a wall peak temperature interval of $T_{wall,max} \approx 950-1000$ K). This mean temperature range, obtained for the hottest tubes, is considered rather conservative because it is assumed that all receiver tube surfaces (A_R) are at these temperatures at any instant of time considered in TMY. For comparison, DELSOL3 assumes an average wall temperature of 753 K (Kistler, 1986) whereas a recent analysis (Rodriguez-Sanchez et al., 2015) of the Solar Two receiver estimates that maximum wall temperatures can reach 595 °C (868 K).

Finally, with respect to the mixed convective coefficient h_{mix}, the individual convection thermal losses at the design point in Gemasolar are also reported (Lata et al., 2006). With the former average wall temperature T_{wall} and assuming reasonable Gemasolar receiver area values, mixed convective coefficients could be estimated from the convective losses in Eq. (4). Therefore, $h_{mix} = 16.61-19.3$ (W/m^2 K). By way of comparison, with an average wall temperature of 753 K, DELSOL3 (Kistler, 1986) suggests that $h_{mix} \approx 15$ W/m^2 K.

Logically, facing the level of uncertainty of the former analysis, all these data should be treated with care.

Fig. 4 shows the calculated annual receiver efficiencies, Eq. (4), which depend on the tested receiver radius, although for only one tower height, THT = 140 m. For example, with a receiver radius of 4.50 m, $\eta_{rec} = 88.05\%$. By way of comparison, Pacheco et al. (2000) report a measured η_{rec} of 88% with low wind velocities and 86% in high wind speeds during receiver efficiency tests at Solar Two (10 MWe). The molten salt receiver in this plant was a cylinder, 5.10 m in diameter and 6.20 m high, with a solar absorptance of 0.95 (Pacheco et al., 2000; Pacheco, 2002).

3.3. Annual absorbed energy efficiency η_{abs}

The annual absorbed energy E_{abs}, can now be related to the annual direct solar energy E_{DNI}, Eq. (1),

$$E_{abs} = \eta_{rec}E_{inc} = (\eta_{rec} \times \eta_{field})E_{DNI} = \eta_{abs}E_{DNI} \Rightarrow \eta_{abs}$$
$$= \eta_{rec} \times \eta_{field} = \frac{E_{abs}}{E_{DNI}}, \tag{6}$$

where η_{abs} is the annual averaged efficiency of the energy the molten salts absorb at the receiver.

In Fig. 4, the lower set of curves stands for η_{abs} versus the receiver radius RR depending on THT. They exhibit a maximum of around $RR = 4.50$ m for the five tower heights. This could be justified by the well-known area receiver field efficiency trade-off (Pitman and Vant-Hull, 1985), because the larger the receiver, the higher the field efficiency, but also the higher the thermal losses. When the increase in field efficiency due to a larger receiver is offset by rising thermal losses, the result is a maximum η_{abs}.

However, given that these energy maxima are rather flat, decreasing the receiver size could be justified due to its high capital cost. In conclusion, capital cost models keep on being essential to define the optimum design of the plant.

3.4. Net annual energy output E_E

Finally, to arrive at the net annual electric output E_E, E_{abs} is multiplied by a set of constant annual averaged efficiency factors $\in_i$, which now, unlike the former efficiencies η, are time independent (Kistler, 1986),

$$E_E = \underbrace{\in_{pip}\in_{sto}\in_{cyc}\in_{aux}\in_{ava}}_{\in_{power}} E_{abs} = \in_{power}E_{abs}$$
$$= \underbrace{(\in_{power} \times \eta_{rec} \times \eta_{field})}_{\eta_{net}} E_{DNI} = \eta_{net}E_{DNI}, \tag{7}$$

where $\in_{pip}$ is the piping insulation losses efficiency, $\in_{sto}$ is the thermal storage efficiency, $\in_{cyc}$ is the thermodynamic efficiency of the steam cycle, $\in_{aux}$ is the auxiliary loads efficiency and, finally, $\in_{ava}$ is the availability factor. In Eq. (7), for the sake of convenience, the product of all these efficiency factors $\in_i$ is called $\in_{power}$, in other words the power block efficiency, whereas the product of the three major efficiencies, η_{field}, η_{abs} and $\in_{power}$, is called the annual averaged net efficiency η_{net}.

Table 1 gathers the $\in_i$ values chosen in this work. By way of example, it also shows the figures for a plant similar to Gemasolar with $RR = 4.00$ m and $THT = 140$ m following the annual energy bookkeeping suggested in Kistler (1986). The power block efficiency is $\in_{power} \approx 0.3032$, which here, as a first approximation, is considered independent from the collector field design. With $\eta_{net} = 0.1587(15.87\%)$, the annual net electric output is $E_E = 0.1587 \times 695.50[\text{GW h}_{th}/\text{year}] = 110.38[\text{GW h}_{el}/\text{year}]$.

By comparison, Gemasolar would be theoretically able to generate $110[\text{GW h}_{el}/\text{year}]$ (Burgaleta et al., 2011). However, note that PSA (Almeria) has been the assumed location of the plant, which has a higher annual DNI (2268 kW h/m^2/year) than the actual Gemasolar location (Seville), 2062 kW h/m^2/year. Consequently, the data used in Table 1 are thought to be rather conservative.

4. LCOE of a power tower plant and selection of the collector field cost models

The LCOE in [¢/kW h$_{el}$] is the plant installed capital cost C_{plant} multiplied by the annuity factor $[i(1+i)^{N_Y}]/[i(1+i)^{N_Y} - 1]$ (Augsburger, 2013), or uniform series capital recovery factor CRF

Table 1
Annual efficiency in a Gemasolar-like plant. Example for (RR = 4 m, THT = 140 m).

DNI Almería (assumed location)	2268 kW h/m²/year Meinecke, 1982
Heliostat field size	2650 *Hel* × 115.72 m²/heliostat = 306,658 m² (Burgaleta et al., 2011)
Annual Direct Solar Energy, E_{DNI}	**695.50 GW ht**
Reflectivity	$\rho = 0.88$ Collado and Guallar, 2013
Cleanliness	0.95 Collado and Guallar, 2013
Field efficiency (η_{field})	58.71%
Annual Incident Energy, E_{inc}	**408,33 GW ht**
Maximum wall receiver temperature (Vázquez et al., 2006; Burgaleta et al., 2011)	950 K
Receiver efficiency (η_{rec})	89.16%
Absorbed energy efficiency (η_{abs})	$\eta_{abs} = \eta_{field} \times \eta_{rec} = 52.35\%$
Annual Absorbed Energy, E_{abs}	**364.07 GW ht**
Piping thermal losses efficiency	$\in_{pip} = 0.99$ (Kistler, 1986)
Storage thermal losses efficiency	$\in_{sto} = 0.995$ (Pacheco, 2002)
Thermodynamic cycle efficiency (annual average)	$\in_{cyc} = 0.38$ (Ortega et al., 2006)
Auxiliary efficiency (high capacity factor)	$\in_{aux} = 0.90$ (Pacheco et al., 2000)
Availability efficiency (high availability)	$\in_{ava} = 0.90$ (Kolb, 2011)
Power Block Net Efficiency	$\in_{power} = \in_{pip} \times \in_{sto} \times \in_{cyc} \times \in_{aux} \times \in_{ava} = 0.3032$
Net Annual Electric Output, E_E	**110.38 GW h$_e$**
Net efficiency	$\eta_{net} = \eta_{field} \times \eta_{rec} \times power = 15.87\%$

In bold, annual energy breakdown following the efficiencies of the different subsystems.

(Siva Reddy et al., 2013), where i is the yearly nominal interest of the loan issued for the total plant investment, and N_Y is the number of years in the plant lifetime. It is then divided by the net annual electric output E_E[kW h$_e$]. The cost of operation and maintenance OM[¢/kW h$_e$] is finally added to the former ratio.

For the sake of simplicity, the insurance cost is left aside and may be considered as included within the yearly nominal interest rate, which according to (Augsburger, 2013) is set at $i = 0.09(9\%)$. The lifespan is assumed $N_Y = 25$ years. Thus, in this work, $CRF = 0.1018$ and the $LCOE$ equation used remains as

$$LCOE[\text{¢/kW h}_e] = \frac{\frac{i(1+i)^{N_Y}}{i(1+i)^{N_Y}-1}C_{plant}}{E_E} + OM = \frac{CRF \times C_{plant}}{E_E} + OM$$
$$= \frac{0.1018 \times C_{plant}}{E_E} + OM. \qquad (8)$$

This recovery factor is similar to the factor used in Avila-Marin et al. (2013), $CRF = 0.0988$, although the latter uses $i = 8\%$, an annual insurance rate of 1%, 30 years of plant life time and 100 MW$_e$ of power. Another analysis (Kolb, 2011) works with a lower fixed charge rate (FCR), equivalent to CRF, of 0.075, but includes tax incentives and a time span of 30 years. Finally, recent IRENA studies (IRENA, 2012; IRENA, 2013) assume a 10% rate of interest and 25-year economic life.

Table 2 depicts the equipment that has been considered at the plant, in addition to its installed cost models. The costs and the $LCOE$ contributions, Eq. (8), are worked out for the same collector field design as in Table 1.

The capital cost of the plant was divided into two main parts: the collector field (basically heliostats, tower and receiver) and the power block.

Table 2
Cost models ($ 2011) used as first option in the LCOE. Example for (RR = 4 m, THT = 140 m).

	Cost model	Gemasolar value	Capital cost ($M)	LCOE (¢/kW h$_e$): Eq. (8)
Land	$1.25/m² (Augsburger, 2013)	1.85 km² (Burgaleta et al., 2011)	2.31	0.21
Improvement	$20/m²-mirror (Kolb, 2011)		6.13	0.57
Heliostat field	$200/m² (Kolb, 2011; Augsburger, 2013)	306,658 m² (Burgaleta et al., 2011)	61.33	5.66
Receiver radius	SAM (Turchi and Heath, 2013), Eq. (10)	4 m (assumed)	26.98	2.49
Tower height	WorleyParsons (Turchi and Heath, 2013), Eq. (9)	140 m (Burgaleta et al., 2011)	25.96	2.39
Install. Collector Field Cost			**122.71**	**11.32**
Thermal storage (15 h)	$30/kW h$_t$ (Kolb et al., 2011)	740 MW h$_t$ (Relloso and Lata, 2011)	22.20	2.05
Steam generation	$350/kW$_e$ (Kolb et al., 2011)		6.97	0.64
Power block	$1000/kW$_e$ (Kolb et al., 2011)	19.9 MW$_e$ (Burgaleta et al., 2011)	19.90	1.84
Cooling system			9.70 (Augsburger, 2013)	0.89
Master control			1.90 (Augsburger, 2013)	0.18
Direct Capital Power Block Cost			**60.67**	**5.60**
Indirect cost-power block	25% (Kolb, 2011)		15.17	1.4
Install. Capital Power Block Cost			**75.84**	**7.00**
Installed Capital Cost			**198.55**	**18.32**
O&M Cost	5.4 ¢/kW h$_e$ (Ortega et al., 2006; Augsburger, 2013)			5.4
LCOE (¢/kW h$_e$), E_E = 110.38 GW h$_e$ **Installed Cost ($/kW$_e$)= 9977.4**				23.72

In bold, capital cost (and corresponding LCOE) breakdown following the collector field and power block costs.

As the power block costs in (Kolb et al., 2011; Augsburger, 2013) are only direct costs, indirect costs must be added to arrive at installed costs. In this paper, indirect costs are estimated as 25% of the direct costs (Kolb, 2011), which is a conservative percentage compared to other sources, 16.5% in Avila-Marin et al. (2013) or 13% in Siva Reddy et al. (2013).

Next is a brief analysis of the selection of the cost models for heliostats, tower and receiver, which are also the less conventional equipment.

4.1. Installed capital cost of the heliostats C_{hel}($M)

C_{hel}($M) is the cost of the whole installed heliostat field, which is directly related to the installed cost of heliostat per square metre of mirror, C_m($/m^2 - mirror$). Therefore, $C_{hel} = C_m A_m N_{hel}$. Following Sandia (Kolb et al., 2011; Kolb, 2011), C_m for current heliostats within initial commercial projects ($\geqslant$100 MWe) would be about $200/m^2. A slightly lower C_m, $181/m^2, can be found in the NREL system advisor model (SAM) spread sheet (Turchi and Heath, 2013). CSIRO (Hinkley et al., 2011) lowers this cost even more to $A142/m^2$ ($132.4/m^2$), in which A stands for Australian dollars. Finally, a detailed analysis of the heliostat cost breakdown, performed at the EPFL (Augsburger, 2013) gives a C_m of about $204/m^2.

In conclusion, as there is a clear agreement between Sandia estimations (Kolb et al., 2011; Kolb, 2011) and the EPFL analysis (Augsburger, 2013) at C_m = $200/m^2, this is the first option chosen here for the mirror cost. Then, $C_{m,1} = $200/m^2$. As a second option, to explore how severe reductions in current mirror prices could affect the field design, a lower heliostat cost (Kolb et al., 2011; Kolb, 2011) was also explored $C_{m,2} = $120/m^2$.

4.2. Installed cost of the tower C_{tow}($M)

The tower cost model suggested in Augsburger (2013) is that of a reference tower 75 m high made of concrete ($1.6 M), multiplied by a scaling effect, a volume effect and a price index. The resulting correlation is $C_{tow-EPFL}$($M) = $1.6 \times \left(\frac{H_T}{75}\right)^{1.8}$. For the tower height in the Gemasolar plant, which is around THT = 140 m (Burgaleta et al., 2011), $C_{tow-EPFL}$ = $4.92 M. By comparison, the tower cost for the baseline case (100 MWe) in Kolb et al. (2011) is $11.75 M, but the tower height is not reported. However, $H_T \approx$ 203 m could be assumed, as it is the reference tower height for the SAM spread sheet (Turchi and Heath, 2013). Inserting $H_T \approx$ 203 m in the former EPFL correlation, the cost would be $9.61 M. However, the cost of this reference tower (203 m high) in SAM (Turchi and Heath, 2013) amounts to $28.5 M (2010), nearly three times the former cost suggested by Sandia in Kolb et al. (2011). Note that the SAM installed tower cost does include riser and down comer pipes and insulation, which add up to $7.1 M. For the 140-m Gemasolar tower, using the above SAM reference tower (203 m) cost of $29.15 M (2011) and the reported size scaling exponent (0.0113) (Turchi and Heath, 2013), it would cost about $29.03 M, although the rather low cost difference between the 140-m and 203-m towers does not seem reasonable.

Finally, in the NREL-SAM report (Turchi and Heath, 2013), Appendix H supplies the following correlation, developed by WorleyParsons, for a concrete tower cost depending on tower optical height (THT),

$$C_{tow-WP}(\$M) = 0.0018357 \times THT^2 - 0.285868 \times THT + 30. \quad (9)$$

With this correlation, the SAM reference tower would now cost $47.61 M, about $18 M higher than the SAM spread sheet value, and more than four times the cost suggested in Kolb et al. (2011).

The Gemasolar tower would now cost $25.96 M. This quadratic interpolation includes the installed tower cost for three heights, 122 m, 178 m and 217 m, which covers the tower height range analysed in this paper, 120–160 m.

In conclusion, given WorleyParsons' experience in renewable energy civil work, the recent publication date (February 2013) of the correlation, the height range covered, and the highly scattered results from other sources, Eq. (9) is the sole tower cost model used here.

The current tower cost uncertainty is far higher than that of the heliostat cost. The Gemasolar tower (140 m) cost would range from $4.92 M, based on the EPFL model (Augsburger, 2013), to $29.03 M, scaled from the SAM spreadsheet data (Turchi and Heath, 2013).

Finally, with Eq. (9), the Gemasolar (20 MWe) tower investment ($25.96 M) is about 42% of the heliostat field cost ($61.33 M). However, for a larger plant, such as the SAM reference case (115 MWe), this percentage would drop to 20% ($47.61 M versus $233.32 M).

4.3. Installed cost of the receiver C_{rec}($M)

For optimisation purposes, the receiver cost should depend on the receiver area. We could use the base receiver cost, $85.1 M, supplied in SAM (Turchi and Heath, 2013) for a project plant (2012) with a reference area receiver of 1133 m^2, which is almost five times larger than Gemasolar. This SAM receiver would have cost $83.34 M in 2011. This installed cost includes horizontal piping and insulation, the cold salt pump, control and instruments and heat trace, and spare parts (Turchi and Heath, 2013).

Using the SAM scale factor for the receiver cost (0.7), the first option for the receiver cost would be:

$$C_{rec-SAM}(\$M) = 83.34 \times \left(\frac{A_R}{1133}\right)^{0.7}. \quad (10)$$

As an alternative, in the EPFL dissertation (Augsburger, 2013), the reference case is the Solar Two receiver, with a heat transfer area of 100 m^2 and $9.1 M of investment (early 1990s). By inserting the volume effect and the price index (Augsburger, 2013), the receiver cost correlation would now be

$$C_{rec-EPFL}(\$M) = 13.09 \times \left(\frac{A_R}{100}\right)^{0.5283} \quad (11)$$

The actual Gemasolar receiver area is not reported in open literature. For example, in Avila-Marin et al. (2013), the receiver area is merely assumed to be 300 m^2.

So, for the reference case used in Table 2, namely RR = 4.00 m, A_R would be 226.20 m^2, the SAM receiver cost, Eq. (10), would amount to $26.98 M. This A_R would be 2.3 times larger than Solar Two's. The EPFL receiver cost model, Eq. (11), for the same A_R would deliver a cheaper receiver of about $20.15 M, almost $7 M less than the SAM model. Therefore, it would seem reasonable to check both receiver cost models, Eqs. (10) and (11) through optimisation.

The Gemasolar tower cost ($25.96 M) calculated with WorleyParsons' correlation would be similar to the receiver cost of the SAM model, Eq. (10), and even more expensive than the receiver cost of the EPFL model, Eq. (11). Along the same lines, but for a 100 MWe plant, CSIRO reports (Hinkley et al., 2011) that the tower ($A14.5 M) is far more expensive than the receiver ($A9.7 M).

4.4. Breakdown of the installed capital cost of the plant and of the LCOE

Table 2 depicts the above first option cost models for the collector field equipment, and also shows the capital costs of the plant's

various elements, for example ($RR = 4$ m, $THT = 140$ m), whose optimised layout can be seen in Fig. B.2 in Appendix B. The total installed cost is $198.55 M, whose 61.8% is the installed collector field. The installed kW results in $9977.4, which is comparable with the $10520 ($2010) Fitchner suggested (Fitchner, 2010) for a power tower with 15 h of molten salt thermal storage (such as Gemasolar).

For the LCOE of solar tower plants (50–100 MW$_e$) with 12–15 h of storage, IRENA estimations (IRENA, 2012, 2013), based on its own sources and on (Turchi and Heath, 2013; Hinkley et al., 2011; Fitchner, 2010), ranged from around 17.00 to 24.00−29.00 ¢/kW he in 2011/2012. Apart from cost uncertainties, this broad range is justified because the LCOE depends primarily on capital costs and the local solar resource (IRENA, 2013), which are highly dependent on location.

Thus, the final LCOE found here (see Table 2) for a Gemasolar-like plant (20 MWe), 23.72 ¢/kW he, would logically be closer to the higher end of that range due to its comparatively low nominal power.

Furthermore, the OM cost used here, 5.4 ¢/kW he, is rather high, more than a fifth of the LCOE, see Table 2. In (IRENA, 2013), the OM cost of CSP plants ranges from ¢2 to ¢3.5/kW he. Plant size clearly affects this cost. Finally, discounting OM costs, the rest of the LCOE figure is 18.32 ¢/kW he, where almost two thirds is for the collector field (11.32 ¢/kW he).

5. LCOE results for a Gemasolar-like solar tower plant

After defining the cost models (Table 2) of the main plant equipment, the sensitivity of the LCOE, Eq. (8), can be plotted against the main design parameters for the twenty-five design options explored (Section 3) here. This is the main optimisation.

5.1. LCOE and NPV versus receiver radius for expensive heliostats and expensive receiver

Fig. 5a shows the LCOE − RR profiles found for the five analysed tower heights. The profile is quite clear and gives well-defined minima for the various options. Therefore, for the cost models in Table 2, which are considered the most probable scenario, in other words expensive heliostats ($200/m²) and expensive receiver (SAM model), the optimum design for the Gemasolar plant
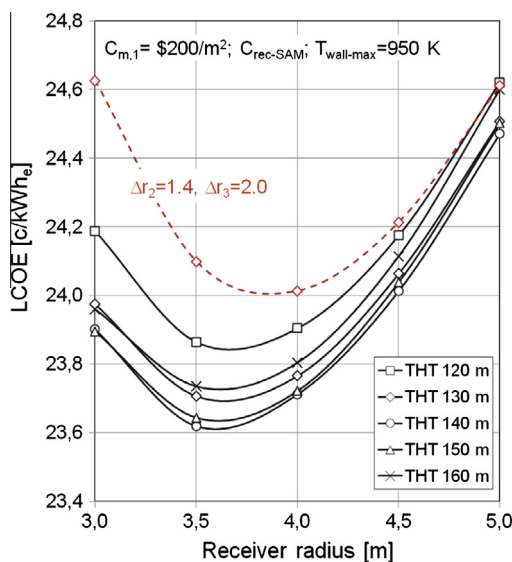
giving the lowest LCOE (about 23.6 ¢/kW he) would be $RR = 3.5 − 3.6$ m and $THT = 140$ m.

The dashed curve stands for the preliminary optimum layout found in Collado and Guallar (2013), which is shown in Fig. B.1 in Appendix B. This weak layout optimisation was more expanded in zone 2 ($\Delta r_2 = 1.4$) than the actual maximum found in this work for ($RR = 3.5$ m, $THT = 140$ m), namely ($\Delta r_2 = 1.00$), see Table B.1, whose layout is shown in Fig. B.3. Although, the absolute difference between field efficiencies was low and around 0.7% (see Figs. B.1–B.3), the optimum design for the expanded layout has a rather different result, $RR = 3.9$ m and $THT = 130$ m. Also, its minimum LCOE (around 24 ¢/kW he) is a little higher than the refined layout optimisation, around 0.4 ¢/kW he.

When several distinct projects are compared with each other, other financial indicators, such as the net present value (NPV), are used (Augsburger, 2013). The NPV is the sum of the updated values of all expenses and incomes over the project lifetime. Thus, the NPV expression is given by the discounted income minus the current value of plant investment (Augsburger, 2013):

$$NPV[\$M] = \frac{i(1+i)^{N_Y} - 1}{i(1+i)^{N_Y}}(ToE - OM)E_E - C_{plant}$$

$$= \frac{i(1+i)^{N_Y} - 1}{i(1+i)^{N_Y}}(ToE - LCOE)E_E, \qquad (12)$$

where Eq. (8) has been included and ToE is the electricity sale price or tariff of electricity. This sale price may be a feed-in tariff (FiT) the authorities define to promote the development of solar thermal plants. For example, a Spanish royal decree assured a FiT of 34(¢/kW he) guaranteed over 25 years (Augsburger, 2013).

Fig. 5b shows the NPV − RR profiles found for the five analysed tower heights for ToE = 34(¢/kW he). This high FiT causes the optimum receiver radius and the tower height to shift towards higher values (around $RR \approx 3.9$−4 m, $THT \approx 160$ m) in relation to the former LCOE minima (around $RR \approx 3.5$−3.6 m, $THT \approx 140$ m), since earnings rise when there is a higher annual electricity production associated with a larger receiver, and a taller tower offsets the increment in receiver and tower capital costs, and higher thermal losses.

In Fig. 5b, the economic losses over the project lifetime of the old weak layout optimisation (Collado and Guallar, 2013) in relation to the refined layout presented here are clearer. The optimum NPV for the weak layout (dashed lines) is around $106 M, whereas that of the refined layout is about $113 M.
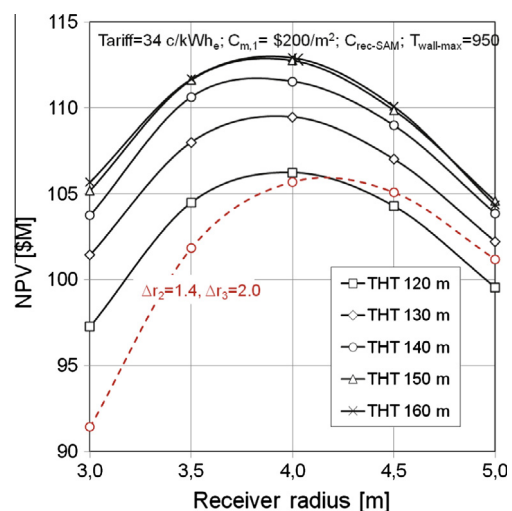

Fig. 5a. *LCOE versus receiver radius. Expensive cost models.*

Fig. 5b. *NPV versus receiver radius for ToE = 34 (¢/kW he). Expensive cost models.*

Fig. 5c is similar to Fig. 5b but it uses a low $ToE = 24(¢/kW\,he)$. Obviously, this sale price is in the boundary of profitability causing economic losses for some collector field design including the weak optimised layout (dashed curve). This low ToE drops the optimum receiver radius to the range of around $RR \approx 3.50$ m and the optimum tower height down to $THT \approx 140$ m.

Finally, Fig. 5d shows the NPV versus receiver radius again for a high $FiT = 34(¢/kW\,he)$, but now with a maximum wall receiver temperature of about 1000 K. Comparing Fig. 5d with Fig. 5b, the optimum receiver size is now lower than before, about $RR \approx 3.75$ m, logically due to higher thermal losses. These thermal losses also reduce profits. The NPV is about $6 M lower than in Fig. 5b ($T_{wall-max} = 950$ K).

5.2. LCOE and NPV versus receiver radius for cheap heliostats and cheap receiver

To again demonstrate the influence of cost model uncertainties on design, Fig. 6a presents the LCOE versus receiver radius for cheap heliostats ($C_{m,2} = \$120/m^2$) and a cheaper receiver, namely the EPFL model, Eq. (11). This figure is compared with Fig. 5a.

First, the new LCOE has fallen almost three cents, obviously due to the huge reduction in mirror cost and the moderate drop in receiver cost. Second, the optimum receiver radius is now
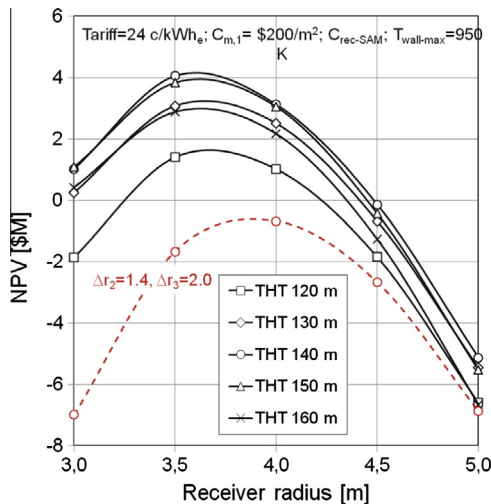

Fig. 6a. LCOE versus receiver radius. Cheap cost models.
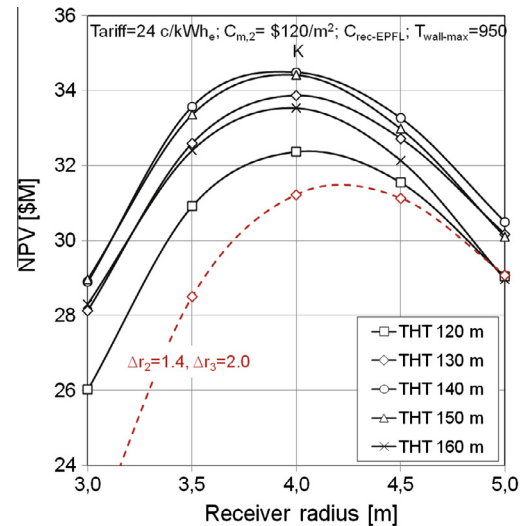
Fig. 6b. NPV versus receiver radius for $ToE = 24$ (¢/kW he). Cheap cost models.

Fig. 5c. NPV versus receiver radius for $ToE = 24(¢/kW\,he)$. Expensive cost models.

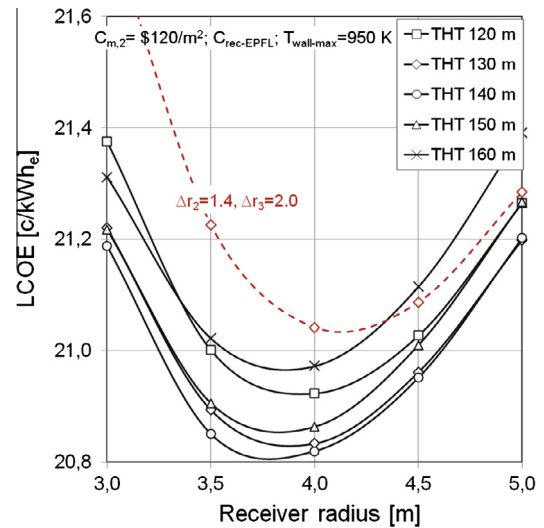**Fig. 5d.** NPV versus receiver radius for $T_{wall-max} = 1000$ K. Expensive cost models.

$RR \approx 3.75$ m, whereas it was $RR \approx 3.5-3.6$ m with expensive receivers. And third, expensive receivers cause taller towers to somehow offset the reduction in energy collection due to a small receiver resulting from a high cost. In Fig. 6a the optimum height for cheap receivers is clearly 140 m, whereas in Fig. 5a the optima are between 140–150 m.

Finally, Fig. 6b shows the NPV versus the receiver radius but now with a low $ToE = 24$ ¢/kW he. This figure should be compared with Fig. 5c. The NPV is positive for all the cases explored, unlike in Fig. 5c, which is clearly due to the drop in investment. Again, but now more defined, working with a cheap receiver involves larger optimum receivers ($RR \approx 4$ m). Working with the NPV, it would seem that the optimum tower height should be a little taller than the optimum found plotting the LCOE versus RR.

6. Discussion and conclusions

Until the knowledge of the authors, this paper presents, by the first time, the thermo-economic optimisation of the collector field (layout for a fixed number of heliostats N_{hel}, tower height THT and receiver dimension RR) of a commercial solar tower plant

(Gemasolar, 20 MWe, surrounding field) based on a detailed performance analysis of the heliostat field (heliostat by heliostat).

One of the main novelties is the achievement of LCOE profiles sharp enough to establish clear minima, at difference from classic codes as DELSOL3, whose profiles are shallow.

Other of the major novelties of the work is the phased optimisation procedure followed, which is based on splitting the full process into two simpler ones. The first step, or primary optimisation, is the energy optimisation of the layout (maximum annual energy) for any pair of the basic field design variables (THT, RR) included in the optimisation. Next, the main optimisation seeks the lowest LCOE (net annual energy-levelised cost ratio) for all the design options checked, in which the annual incident energy on the receiver is already a maximum.

The clear advantage of this simple two steps optimisation approach (based on parametric analysis) over any advanced global search algorithm (such as genetic ones) would be a better definition of the search space. Since the interval of variation of the design variables, their increment step sensitivity, and their relative importance in regard to $LCOE$ have been assessed through this analysis. Without this parametric study, the global advanced search would be, in some manner, "blind".

So, it has been possible to find $LCOE$ profiles with well-defined minima using twenty-five basic combinations of field design variables, namely $RR(m) = [3.0, 3.5, 4.0, 4.5, 5.0] \times THT(m) = [120, 130, 140, 150, 160]$, in which their associated heliostat layout fields have been previously optimised.

Along the same lines, brand new layouts have been proposed, which clearly improve the field efficiency with regard to old layouts presented elsewhere (Collado and Guallar, 2013). Campo, as with other modern layout codes, is able to define the entire field layout through only a few variables, namely $(\Delta r_2, \Delta r_3)$, which are the non-dimensional radial increments in zones 2 and 3. The new layouts are denser in the central zone 2 and a little more expanded in zone 3.

Hence, nine brand new layout designs have been successfully proven for each of the above twenty-five design combinations in particular, $\Delta r_2 = [1.0, 1.1, 1.2] \times \Delta r_3 = [2.0, 2.2, 2.4]$.

Furthermore, the first optimisation stage i.e., the layout energetic one, has allowed to find that the optimal distributions practically do not depend on Δr_3 in the above explored interval, see Fig. 1. This would mean one design variable less to deal with in the search space.

One of the key points of this two-stages optimisation is to keep N_{hel} constant for all the explored combinations (THT, RR), thus ensuring that the capital cost of each analysed design option does not change along the energy search. Therefore, after layout modifications, land investment changes and cost variations of heliostat wiring are considered negligible. As the number of heliostats is closely related to the power of the plant, this process would be similar to the optimisation of a solar tower plant with a prescribed nominal power.

The optimal layouts found in this work (giving maximum annual incident energy) are shown in Table B.1 whereas the relevant maximum field efficiencies are depicted in Fig. 4. The boundary of the field, defined at the same time as the optimised layout, is also a major result of this primary optimisation.

Notice that Δr_1, which is the radial increment for the first zone (closest to the tower), has been kept to the minimum value in all cases, $\Delta r_1 = \cos 30° = 0.866$, besides the number of heliostats in the first row $Nhel_1 = 46$. Strictly speaking, $Nhel_1$ should have been included in the set of layout design variables as well. However, with DM = 15.70 m, 46 tangent heliostats make a first row circle with a radius equal to 115 m, which is equal to 0.82×140 m. This is close to the DELSOL3 reference value for this first row of

$0.75 \times THT$. Therefore, for the sake of reducing the large number of cases to be worked out, $Nhel_1$ has been set to a value close to the optimum reference proposed by DELSOL3.

Besides, it has not been necessary to add any additional security $(dsep = 0)$ because the optimal layouts for zone 1 are the densest ones; in zone 2, the new layouts suggested here are significantly denser than the old designs explored elsewhere (Collado and Guallar, 2013), in which $dsep = 0$ too; and, finally, in zone 3, the optimal distributions resulted practically independent of the radial distance between consecutive rows.

The calculation of the net annual energy in the LCOE in this paper is merely the multiplication of the maximum annual incident energy by annual averaged values of the power block efficiency and of the receiver thermal losses. The latter are strongly based on an effective wall temperature.

Clearly, the receiver wall temperature is not at all constant over the receiver surface or along the TMY. However, an exact calculation of annual thermal losses would imply, firstly, solving the instantaneous wall temperature map and the energy absorbed by the molten salts. As an input, this would not only need the instantaneous flux map sent by the heliostat field, but also the detailed receiver design. Secondly, this process should be repeated for any time instant throughout any day included in the TMY to obtain the annual absorbed energy.

This laborious annual calculation should also be repeated 25×9 times (the collector designs scanned) not only for annual thermal losses but also for the auxiliary efficiency $\in_{aux}$, included in the power block efficiency Eq. (7). This is due to the power consumption of the molten salts pump, because the higher the molten salts velocity in the tubes, the lower the surface temperature, but higher the pressure drop.

Although this huge computational effort would be technically possible, it is doubtful that it would be worthwhile due to the uncertainties of the receiver cost models commented on later. As a reasonable alternative, a conservative range of the effective wall temperature was selected in this work. Here, an annual average mean receiver wall temperature was approximately derived for the hottest tubes based on the assumed maximum wall temperature range, which, in turn, was estimated from preliminary thermal–hydraulic analysis (Lata et al., 2006).

In conclusion, derived from scarce information in Lata et al. (2006), the receiver maximum wall temperature chosen was assumed to be 950 K. Nevertheless, 1000 K was also checked throughout the LCOE optimisation. Therefore, the effective wall temperature range used to arrive at the annual absorbed energy was $T_{wall} \approx 813 - 863$ K, which is about 100 K greater than the wall temperature used in DELSOL3 (750 K), although this is not far from the effective temperature (790 K) calculated in Rodriguez-Sanchez et al. (2015) for the Solar Two receiver.

On the other hand, the review of the capital costs of the major components of the collector field clearly show that the receiver and tower investment costs are more uncertain than the mirror cost, at least in the open literature.

The cost of today's installed heliostats would be about $200/m^2$ per mirror, confirmed by Sandia (Kolb et al., 2011; Kolb, 2011) and EPFL (Augsburger, 2013). Moreover, the cost suggested by the System Advisor Model (SAM-NREL) (Turchi and Heath, 2013) is similar, $181/m^2$ per mirror. However, the current receiver cost is more uncertain. For example, the installed cost of a receiver for a commercial scale plant (>100 MWe), with a heat surface of $1133 m^2$, would range from $83.34 M in SAM (Turchi and Heath, 2013) to $47.2 M using an EPFL correlation (Augsburger, 2013).

Even the tower cost is more uncertain than the mirrors'. For example, the cost of a 203 m height tower, which would be the reference value for a commercial plant (Turchi and Heath, 2013),

ranges from $11.75 M in 2011 Sandia reports (Kolb et al., 2011; Kolb, 2011) to $28.5 M in SAM (2013) (Turchi and Heath, 2013). However, this 203 m tower would cost $47.61 M now using the recent WorleyParsons correlation (Turchi and Heath, 2013).

The SAM-NREL (Turchi and Heath, 2013) application is considered the most serious attempt to update and establish reasonable installed cost models for the major equipment of solar tower power plants in the commercial range (>100 MW$_e$). In this paper, the receiver cost model is scaled through the SAM-NREL data, the tower cost uses the WorleyParsons correlation, but the mirror cost has been set to $200/m^2.

For a solar tower plant with 15 h of storage, such as Gemasolar (around 20 MWe), and using the PSA-Almeria solar resource (Meinecke, 1982), the LCOE would be around 24 ¢/kW he ($2011). This cost is in the higher-end range that IRENA recently reported (IRENA, 2012, 2013). However, in these reports, the plants are in the 50–100 MWe range.

As a consequence of the above, this LCOE figure should be treated with extreme care because scale economies in much larger plants could drastically lower this cost. Furthermore, the operation and maintenance (OM) cost used in this work, 5.4 ¢/kW he Lata et al., 2006; Augsburger, 2013, is rather high compared with those reported in IRENA, 2012, 2013, namely 2—3.5 ¢/kW he. Finally, two thirds of the remaining cost, 18.6 c/kW h, after discounting the OM costs from the LCOE, is for the collector field. This merely confirms the well-known importance of the collector field in cost reduction (Kolb et al., 2011; Kolb, 2011).

Lastly, concerning the result of the main or economic optimisation, the LCOE (or the NPV) plots versus the receiver radius for the different tower heights explored are acute enough to easily establish optima, thus supplying definite selection criteria. Furthermore, assessing the sensitivity of the optimum designs to several changes was possible in both the cost models and the annual energy calculation. It has been clearly verified that preliminary optimised layouts supply rather worse economic results than refined optimised layouts.

For the various cost options and financial indicators used, the optimum RR ranges between 3.50 and 4 m, whereas the optimum tower optical height (THT) ranges from 140 to 160 m. These values are in reasonable agreement with the scarce information given in the open literature about Gemasolar (Lata et al., 2006; Lata et al., 2010).

Annual thermal losses at the receiver play a major role in the main optimisation process. An increase in the assumed maximum wall temperature of the receiver clearly reduces not only the optimum size but also the benefits. Thus, the reasoned optimum selection of the maximum wall temperature is a task ahead, which should include heat transfer and pressure drop models, in addition to molten salt pump consumption. However, the uncertainty of the cost models is high enough to compensate such assumptions, as it arises from the difference between expensive and cheap cost models.

A reasonable conclusion about the final design of the receiver and its thermal losses (with optimal layouts already designed) could be to analyse the thermal–hydraulics in depth, but only for two receiver sizes, RR = 3.5 m and RR = 4.0 m, to obtain accurate annual thermal losses and molten salt pump consumptions. This, combined with cost models, would allow for a more accurate LCOE calculation. Moreover, for RR = 3.50–4 m and THT = 140–160 m, the layouts have similar designs, see Table B.1. The current layout optimisations would not then have to be repeated. In this way, the complex entire design problem would be structured in several more manageable subtasks. For example, the problem of the maximum flux and the heliostat aiming strategy (Besarati et al., 2014) should be done at this final stage of the design process.

Apart from the cost models and the maximum wall temperature, the most influential parameter in the collector field design would be the tariff of electricity (ToE). For example, with a high ToE, due to a feed-in tariff (FiT), it is profitable to use larger receivers and taller towers, in spite of higher investments and higher thermal losses. Consequently, a stable and predictable regulatory framework of the electricity market would greatly help the development of solar tower power technologies.

Conflict of interest

The authors declare that there is no actual or potential conflict of interest including any financial, personal or other relationships with other people or organizations within three years of beginning the submitted work that could inappropriately influence, or be perceived to influence, their work.

Acknowledgments

Appendices A&B. Supplementary material

Supplementary data associated with this article can be found, in the online version, at http://dx.doi.org/10.1016/j.solener.2016.06.065.

References

Atif, M., Al-Sulaiman, F.A., 2015. Optimization of heliostat field layout in solar central receiver systems on annual basis using differential evolution algorithm. Energy Convers. Manage. 95, 1–9.

Augsburger. G., 2013. Thermo-economic optimisation of large solar tower power plants. Thèse N° 5648, EPFL. Lausanne, Switzerland.

Avila-Marin, A.L., Fernandez-Reche, J., Tellez, F.M., 2013. Evaluation of central receiver solar power plants: configuration, optimization and trends. Appl. Energy 112, 274–288.

Besarati, S.M., Goswami, D.Y., 2014. A computationally efficient method for the design of the heliostat field for solar power tower plant. Renew. Energy 69, 226–232.

Besarati, S.M., Yoswami, D.Y., Stefanakos, E.K., 2014. Optimal heliostat aiming strategy for uniform distribution of heat flux on the receiver of solar power plant. Energy Convers. Manage. 84, 234–243.

Boehm, R.F., 1986. Review of thermal loss evaluations of solar central receivers. SAND85-8019.

Burgaleta, J.I., Arias, S., Ramírez, D., 2011. Gemasolar, the first tower thermosolar commercial plant with molten salt storage. In: Proceedings SolarPACES, Granada, Spain.

Collado, F.J., 2010. One-point fitting of the flux density produced by a heliostat. Sol. Energy 84, 673–684.

Collado, F.J., Guallar, J., 2012. Campo: generation of regular heliostat fields. Renew. Energy 46, 49–59.

Collado, F.J., Guallar, J., 2013. A review of optimized design layouts for solar power tower plants with campo code. Renew. Sustain. Energy Rev. 20, 142–154.

Fitchner, 2010. Technology assessment of CSP technologies for a site specific project in South Africa final report. The World Bank and ESMAP, Washington, DC.

Hinkley, J., et al., 2011. Concentrating solar power-drivers and opportunities for cost-competitive electricity. CSIRO Report.

Ho, C.K., Iverson, B.D., 2014. Review of high-temperature central receiver designs for concentrating solar power. Renew. Sustain. Energy Rev. 29, 835–846.

Ho, C.K., Mahoney, A.R., Ambrosini, A., Bencomo, M., Hall, A., Lambert, T.N., 2014. Characterization of Pyromark 2500 paint for high-temperature solar receivers. J. Solar Energy Eng. 136, 014502.

International Renewable Energy Agency (IRENA), 2012. Renewable energy technologies cost analysis series: Volume 1 power sector (issue 2/5): Concentrating Solar Power.

International Renewable Energy Agency (IRENA), 2013. Renewable power generation costs in 2012: an overview.

Kistler, B.L., 1986. A user's manual for DELSOL3: a computer code for calculating the optical performance and optimal system design for solar thermal central receiver plants. SAND86-8018.

Kolb, G.J., 2011. An evaluation of possible next-generation high-temperature molten-salt power towers. SAND2011-9320.

Kolb, G.J., Ho, C.K., Mancini, T.R., Gary, J.A., 2011. Power tower technology roadmap and cost reduction plan. SAND2011-2419.

Lata, J., Rodríguez, M., Álvarez de Lara, M., 2006. High flux central receivers of molten salts for the new generation of commercial stand-alone solar power plants. In: Proceedings SolarPACES, Sevilla, Spain.

Lata, J., Alcalde, S., Fernández, D., Lecube, X., 2010. First surrounding field of heliostats in the world for commercial solar power plants-Gemasolar. In: Proceedings SolarPACES, Perpignan, France.

Lipps, F.W., Vant-Hull, L.L., 1978. A cellwise method for solar central receivers systems. Sol. Energy 20, 505–516.

Meinecke, W., 1982. IAS-RL-100200-028, Almería, Spain.

Noone, C.J., Torrilhon, M., Mitsos, A., 2012. Heliostat field optimization: a new computationally efficient model and biomimetic layout. Sol. Energy 86, 792–803.

Obitko, M., 2016. <http://www.obitko.com/tutorials/genetic-algorithms/index.php>.

Ortega, J.I., Burgaleta, J.I., Téllez, F.M., 2006. Central receiver system (CRS) solar power plant using molten salt as heat transfer fluid. In: Proceedings SolarPACES, Sevilla, Spain.

Pacheco, J.E., 2002. Final test and evaluation results from the solar two project. SAND2002-0120.

Pacheco, J.E., Reilly, H.E., Kolb, G.J., Tyner, C.E., 2000. Summary of the solar two: test and evaluation program. SAND2000-0372C.

Pitman, C.L., Vant-Hull, L.L., 1985. Receiver loss study; optics of optimized solar central receiver systems as a function of receiver thermal loss per unit area. SAND85-8176.

Relloso, S., Lata, J., 2011. Molten salt thermal storage: a proven solution to increase plant dispatchability. Experience in Gemasolar tower plant. In: Proceedings SolarPACES, Granada, Spain.

Rodriguez-Sanchez, M.R., Sanchez-Gonzalez, A., Santana, D., 2015. Revised receiver efficiency of molten-salt power towers. Renew. Sustain. Energy Rev. 52, 1331–1339.

Sánchez, M., Romero, M., 2006. Methodology for generation of heliostat field layout in central receiver systems based on yearly-normalized energy surfaces. Sol. Energy 80, 861–874.

Sassi, G., 1983. Some notes on shadow and blockage effects. Sol. Energy 31, 331–333.

Schmitz, M., Schwarzbölz, P., Buck, P., Pitz-Paal, R., 2006. Assessment of the potential improvement due to multiple apertures in central receiver systems with secondary concentrators. Sol. Energy 80, 111–120.

Schwarzbölz, P., Schmitz, M., Pitz-Paal, R., 2009. Visual HFLCAL – a software tool for layout and optimization of heliostat fields. In: Proceedings SolarPACES, Berlin, Germany.

Siva Reddy, V., Kaushik, S.C., Ranjan, K.R., Tyagi, S.K., 2013. State-of-the-art of solar thermal power plants – a review. Renew. Sustain. Energy Rev. 27, 258–273.

SolarPACES, 2016 <http://www.solarpaces.org/csp-technology/csp-projects-around-the-world>.

Turchi, C., Heath, G., 2013. Molten salt power tower cost model for the system advisory model (SAM). NREL/TP-5500-57625 (free download at <https://sam.nrel.gov/cost>).

Vázquez, J., Relloso, S., Domingo, M., Valverde, A., Monterreal, R., García, G., 2006. Sener heliostat design and testing. In: Proceedings SolarPACES, Sevilla, Spain.

Wei, X., Lu, Z., Wang, Z., Yu, W., Zhang, H., Yao, Z., 2010. A new method for the design of the heliostat field layout for solar tower power plant. Renew. Energy 35, 1970–1975.